Research Article

Cancer Immunology Research

Poor Response to Neoadjuvant Chemotherapy Correlates with Mast Cell Infiltration in Inflammatory Breast Cancer

Sangeetha M. Reddy[1,2], Alexandre Reuben[3,4], Souptik Barua[5,6], Hong Jiang[3], Shaojun Zhang[7], Linghua Wang[7], Vancheswaran Gopalakrishnan[3], Courtney W. Hudgens[8], Michael T. Tetzlaff[8,9], James M. Reuben[10,11], Takahiro Tsujikawa[12,13], Lisa M. Coussens[12], Khalida Wani[8], Yan He[8], Lily Villareal[11], Anita Wood[11], Arvind Rao[6,14], Wendy A. Woodward[11,15], Naoto T. Ueno[1,11], Savitri Krishnamurthy[11,16], Jennifer A. Wargo[3,7], and Elizabeth A. Mittendorf[17,18,19]

Abstract

Our understanding is limited concerning the tumor immune microenvironment of inflammatory breast cancer (IBC), an aggressive form of primary cancer with low rates of pathologic complete response to current neoadjuvant chemotherapy (NAC) regimens. We retrospectively identified pretreatment ($N = 86$) and matched posttreatment tissue ($N = 27$) from patients with stage III or *de novo* stage IV IBC who received NAC followed by a mastectomy. Immune profiling was performed including quantification of lymphoid and myeloid infiltrates by IHC and T-cell repertoire analysis. Thirty-four of 86 cases in this cohort (39.5%) achieved a pathologic complete response. Characterization of the tumor microenvironment revealed that having a lower pretreatment mast cell density was significantly associated with achieving a pathologic complete response to NAC ($P = 0.004$), with responders also having more stromal tumor-infiltrating lymphocytes ($P = 0.035$), $CD8^+$ T cells ($P = 0.047$), and $CD20^+$ B cells ($P = 0.054$). Spatial analysis showed close proximity of mast cells to $CD8^+$ T cells, $CD163^+$ monocytes/macrophages, and tumor cells when pathologic complete response was not achieved. PD-L1 positivity on tumor cells was found in fewer than 2% of cases and on immune cells in 27% of cases, but with no correlation to response. Our results highlight the strong association of mast cell infiltration with poor response to NAC, suggesting a mechanism of treatment resistance and a potential therapeutic target in IBC. Proximity of mast cells to immune and tumor cells may suggest immunosuppressive or tumor-promoting interactions of these mast cells.

Introduction

Inflammatory breast cancer (IBC) is an aggressive form of the disease characterized by dermal lymphatic blockage by the tumor mass or tumor emboli, leading to the clinical appearance of inflammation on initial presentation (1). Locally advanced IBC is routinely treated with neoadjuvant chemotherapy (NAC) followed by surgery and radiotherapy; however, these patients experience low pathologic complete response (pCR) rates

[1]Department of Breast Medical Oncology, The University of Texas MD Anderson Cancer Center, Houston, Texas. [2]Department of Internal Medicine, The University of Texas Southwestern Medical Center, Dallas, Texas. [3]Department of Surgical Oncology, The University of Texas MD Anderson Cancer Center, Houston, Texas. [4]Department of Thoracic/Head and Neck Medical Oncology, The University of Texas MD Anderson Cancer Center, Houston, Texas. [5]Department of Electrical and Computer Engineering, Rice University, Houston, Texas. [6]Department of Computational Medicine and Bioinformatics, University of Michigan, Ann Arbor, Michigan. [7]Department of Genomic Medicine, The University of Texas MD Anderson Cancer Center, Houston, Texas. [8]Department of Translational Molecular Pathology, The University of Texas MD Anderson Cancer Center, Houston, Texas. [9]Department of Pathology, The University of Texas MD Anderson Cancer Center, Houston, Texas. [10]Department of Hematopathology, The University of Texas MD Anderson Cancer Center, Houston, Texas. [11]Morgan Welch Inflammatory Breast Cancer Research Program and Clinic, Houston, Texas. [12]Department of Cell, Developmental, and Cancer Biology, Oregon Health and Science University, Portland, Oregon. [13]Department of Otolaryngology-Head and Neck Surgery, Kyoto Prefectural University of Medicine, Kyoto, Japan. [14]Department of Radiation Oncology, University of Michigan, Ann Arbor, Michigan. [15]Department of Radiation Oncology, The University of Texas MD Anderson Cancer Center, Houston, Texas. [16]Department of Breast Surgical Pathology, The University of Texas MD Anderson Cancer Center, Houston, Texas. [17]Department of Breast Surgical Oncology, The University of Texas MD Anderson Cancer Center, Houston, Texas. [18]Division of Breast Surgery, Department of Surgery, Brigham and Women's Hospital, Boston, Massachusetts. [19]Breast Oncology Program, Dana-Farber/Brigham and Women's Cancer Center, Boston, Massachusetts.

Note: Supplementary data for this article are available at Cancer Immunology Research Online (http://cancerimmunolres.aacrjournals.org/).

N.T. Ueno, S. Krishnamurthy, J.A. Wargo, and E.A. Mittendorf contributed equally to this article.

Corresponding Authors: Elizabeth A. Mittendorf, Brigham and Women's Hospital, Breast Oncology Program, Dana-Farber/Brigham and Women's Cancer Center, Yawkey Center, Suite 1220, 450 Brookline Drive, Boston, MA 02115. Phone: 617-582-9980; E-mail: emittendorf@bwh.harvard.edu; Jennifer A. Wargo, Department of Surgical Oncology, The University of Texas MD Anderson Cancer Center, 1515 Holcombe Boulevard, Unit 1484, Houston, TX 77030. Phone: 713-745-1553; E-mail: jwargo@mdanderson.org; Savitri Krishnamurthy, Department of Pathology, The University of Texas MD Anderson Cancer Center, 1515 Holcombe Boulevard, Unit 0053, Houston, TX 77030. Phone: 713-794-5625; E-mail: skrishna@mdanderson.org; and Naoto Ueno, Department of Breast Medical Oncology, The University of Texas MD Anderson Cancer Center, 1515 Holcombe Boulevard, Unit 1354, Houston, TX 77030. Phone: 713-792-8754; E-mail: nueno@mdanderson.org

Cancer Immunol Res 2019;7:1025–35

doi: 10.1158/2326-6066.CIR-18-0619

(~15%) (2) and poor survival outcomes compared with stage matched non-IBC cases (3, 4). *De novo* stage IV patients may also receive NAC followed by aggressive local therapy for palliative purposes given the significant breast discomfort associated with IBC; investigations are ongoing into therapeutic benefit of this strategy that emphasizes local disease control (5, 6). Unfortunately, targeted genomic profiling has provided limited insight into what distinguishes IBC from non-IBC, and molecularly targeted trials have shown limited success.

Immunotherapeutic agents such as monoclonal antibodies targeting immune checkpoints have revolutionized treatment of many types of solid tumors; however, they have shown modest efficacy thus far in breast cancer (7). There remains significant interest in evaluating the role of immune-checkpoint blockade in breast cancer, including IBC. Available data have shown that IBC is associated with upregulated inflammatory pathways (e.g., NF-B, JAK/STAT, IL6, COX-2; ref. 8) and that defects in antitumor immunity may contribute to the tumorigenesis and evolution of IBC (9, 10). In contrast, cytotoxic T-cell responses and associated exhaustion markers such as PD-L1 have been correlated with favorable outcomes in IBC (11, 12). Unfortunately, the majority of published data are based on gene-expression profiling. Therefore, there is a critical need for comprehensive morphologic characterization of immunologic aspects of the IBC tumor microenvironment (TME) and the relation to clinical outcomes.

To address this gap in understanding, this study was undertaken to morphologically characterize immunologic aspects of the IBC TME in a prospectively collected cohort of treatment-naïve locally advanced and *de novo* stage IV IBC patients, and to correlate these features with pathologic response to NAC. In addition to confirming biomarkers of response previously reported in non-IBC patients (tumor-infiltrating lymphocytes, $CD8^+$ T cells), we identified mast cells, a critical regulator of several inflammatory conditions, as strongly associated with poor treatment outcomes. Mast cells represent a potential therapeutic target against which pharmacologic agents already exist, making translation readily accessible for future clinical studies. In addition, these findings provide additional evidence for the "inflammatory" underpinnings of IBC and its poor prognosis.

Materials and Methods

Study oversight

This study was approved by the MD Anderson Cancer Center Institutional Review Board. The study was conducted in accordance with the ethical principles of the Declaration of Helsinki, and the protocol was conducted in compliance with all relevant ethical regulations. Written informed consent was obtained from all participants.

Cohort and tissue selection

Patients with an available hematoxylin and eosin (H&E) slide from pretreatment breast core biopsy tissue were identified in the MD Anderson IBC Tissue Bank. The MD Anderson IBC Tissue Registry was searched to identify which of these patients had stage III or *de novo* stage IV disease and received NAC followed by a mastectomy. The immune analyses of *de novo* stage IV disease were performed on core biopsy tissue from the primary lesion in the breast as opposed to metastatic tissue, facilitating comparisons with stage III disease. Clinicopathologic data were recorded, including age, race, stage, grade, histology, and receptor subtype. Treatment information (including use of chemotherapy, anti-HER2 targeted therapy, and endocrine therapy) and outcome data [including pathologic responses, progression-free survival (PFS), and overall survival (OS)] were also recorded. PFS was computed from the time of surgery to the time of relapse if stage III disease or clinical progression as deemed by the treating physician if stage IV disease or death, and OS from the time of surgery to time of death. Patients were categorized into responder and nonresponder groups for immune profiling (Supplementary Fig. S1). The use of the tissue and clinical data for these studies was covered under a protocol approved by the MD Anderson Institutional Review Board.

Immune profiling

Tumor-infiltrating lymphocyte assessment. From each case, an H&E slide was assessed for tumor-infiltrating lymphocytes (TIL). TILs were enumerated on H&E slides from pretreatment core biopsies according to the International TIL Working Group consensus guidelines (13). TILs were quantified by a breast cancer pathologist as a percentage of stromal area occupied by mononuclear inflammatory cells based on H&E slides.

Singlet IHC staining and quantification

IHC was performed using an automated stainer (Leica Bond Max, Leica Biosystems) staining for CD8 (Thermo, clone C8/144B, catalog no. MS-457-S, 1:20 dilution) and PD-L1 (pharmDx, clone 22C3, 1:40 dilution). Slides were stained using previously optimized conditions with appropriate positive and negative controls. Leica Bond Polymer Refine detection kit and DAB chromagen were used and counterstained with hematoxylin. Slides were scanned into an Aperio slide scanner (Aperio AT Turbo, Leica Biosystems) and analyzed with Aperio Image Toolbox software for $CD8^+$ cell staining. Regions of invasive tumor and associated stroma were chosen for digital analysis, and quantification of cell density (cells/mm^2) was performed. PD-L1 expression was scored as the percentage of positive cells with membranous or cytoplasmic staining pattern (0–100).

Multiplex IHC staining and singlet quantification

Sequential multiplex IHC was performed as previously described (14) using a myeloid panel and a lymphoid panel. Briefly, FFPE tissue sections were deparaffinized, counterstained in hematoxylin, and then the whole slide scanned into an Aperio slide scanner. After blocking with endogenous peroxidase and heat-based antigen retrieval, the slides underwent sequential iterative cycles of blocking with 5% normal goat serum/2.5% BSA/1× PBS, primary antibody incubation, secondary horseradish conjugated antibody incubation with HistoFine (mouse or rabbit) Simple Stain MAX PO (Nichirei Bioscience Inc.) for 30 minutes, and then visualization with 3-amino-9-ethylcarbazole (AEC) detection. The slides were subsequently scanned by Aperio slide scanner after which they were destained with an alcohol gradient, followed by heat-based antibody stripping and antigen retrieval. This cycle was repeated for sequential staining on a single FFPE slide.

The myeloid panel was modified from the original published protocol (14) with the following cycle order, primary antibodies, and incubation times: hematoxylin (Dako S3301, 1 minute), tryptase (AA1, Abcam, 1:20000, blocking 10 minutes, primary

30 minutes, AEC 10 minutes), CD68 (PG-M1, Abcam, 1:50, blocking 10 minutes, primary 30 minutes, AEC 10 minutes), CD8 (C8/144B, Thermo Scientific, 1:25, blocking 20 minutes, primary 30 minutes, AEC 25 minutes), CD163 (10D6, Thermo Scientific, 1:100, blocking 10 minutes, primary 30 minutes, AEC 10 minutes), HLA-DR (SPM288, Novus Biological, 1:100, blocking 10 minutes, primary 30 minutes, AEC 10 minutes), CD3 (SP7, Thermo Scientific, 1:150, blocking 20 minutes, primary 60 minutes, AEC 15 minutes), and cytokeratin (AE1/AE3 1:50, MNF116 1:50, 8 and 18 1:25, blocking 10 minutes, primary 30 minutes, AEC 5 minutes). The lymphoid panel was modified with the following cycle order, primary antibodies, and incubation times: hematoxylin (Dako S3301, 1 minute), CD3 (SP7, Thermo Scientific, 1:150, blocking 20 minutes, primary 60 minutes, AEC 15 minutes), FoxP3 (236A/E7, eBioscience, 1:40, blocking 10 minutes, primary 60 minutes, AEC 20 minutes), CD8 (C8/144B, Thermo Scientific, 1:25, blocking 20 minutes, primary 30 minutes, AEC 25 minutes), CD20 (L26, Agilent DAKO, 1:300, blocking 20 minutes, primary 30 minutes, AEC 10 minutes), CD56 (123C3, DAKO, 1:100, blocking 10 minutes, primary 60 minutes, AEC 15 minutes), and cytokeratin (AE1/AE3 1:50, MNF116 1:50, 8 and 18 1:25, blocking 10 minutes, primary 30 minutes, AEC 5 minutes). Singlet quantification of stains was performed as described above.

DNA extraction

Sections from paraffin-embedded tissue were reviewed for pathologic diagnosis and dissected if necessary to ensure that ≥90% of the sample represented tumor. Total cellular DNA was isolated from tissue sections using the QIAmp FFPE DNA isolation kit according to the manufacturer's protocol (Qiagen Inc.) following deparaffinization and proteinase K treatment.

T-cell receptor (TCR) sequencing and analysis

TCR beta chain CDR3 regions were sequenced by immunoSEQ (Adaptive Biotechnologies), with primers annealing to V and J segments, resulting in amplification of rearranged VDJ segments from each cell. Clonality and richness values were obtained through the Analyzer website. Clonality was measured as 1 − (entropy)/log2(# of productive unique sequences), with entropy taking into account clone frequency.

Cell localization and spatial analysis

Spatial localization. As previously described (14), the images acquired from the multiplex IHC staining were aligned by calculation of xy coordinates of fixed structures within each image and then adjustment was made through CellProfiler. Using ImageJ, these images were converted to gray scale and contrast adjusted to discriminate positive staining from background staining. To quantify the spatial proximities of cells exhibiting the queried markers, candidate nuclei in the hematoxylin IHC-stained slides were identified using the connected component analysis algorithm (15) with the MATLAB function "bwconncomp" (16). Candidates whose diameters were too small or too large to be a cell (<4 μm and >16 μm, respectively) were rejected, and IHC stains of markers were overlaid over the nuclei candidates to determine which cells were positive for each marker.

Spatial G-function. The spatial G-function was used to quantify infiltration of cells of one type into another (17). This technique was used in non–small cell lung cancer and intraductal papillary mucinous neoplasms to quantify the proximities of immune cell types to cancer cells, and shown to have a significant association with OS and risk of tumor progression (18, 19). Used previously in modeling spatial statistics in ecology (20), the G-function $G(r)$ is a nearest-neighbor distribution function that indicates the probability of a cell of type "i" having at least one cell of type "j" within a distance "r" μm. If we denote all cells of type i as X_i and all cells of type j as X_j, then the following equation describes the G-function mathematically:

$$G(r) = \text{Prob}(\rho(x_i, X_j) \leq r)$$

where $\rho(x_i, X_j) = \min(||x_i - x_j||_2 \ : x_j \in X_j)$ is the minimum distance between a cell x_i and cells x_j, and Prob(.) indicates the probability distribution function of the quantity within the bracket.

Consequently, this function rises sharply when cells of types "j" and "i" are clustered together, and sluggishly when the two groups of cells are further away from each other. Thus, the shape of the G-function provides a signature of the infiltration pattern. The G-function can be efficiently and compactly represented by computing (18), the area under the G-function curve (=G-function AUC). The G-function AUC is computed between a distance $r = 0$ and $r = r_{max}$, as a quantitative surrogate of the amount of infiltration of one cell type into another. Various values of r_{max} between 5 and 50 μm were experimented with. The spatial analysis was performed using R's spatstat package (21).

Statistical design

Associations between categorical measures were evaluated using the χ^2 or Fisher exact test as appropriate, whereas differences in continuous measures between groups were tested using the Mann–Whitney U test (if only two groups) or Kruskal–Wallis test (if more than two groups). Correlations between continuous variables were calculated using Spearman rho. Fold change in immune markers with treatment were assessed within each response group using one sample Student t test if sample had normal distribution by Shapiro–Wilk test or Wilcoxon signed-rank test if sample was not normally distributed, with a null hypothesis of 1. PFS and OS were estimated using the Kaplan–Meier method, and differences between groups were assessed using the log-rank test. Comparison of PFS by immune cell infiltration in posttreatment tissue was made between the highest and lowest quartiles of immune cell infiltration. All analyses were performed using GraphPad Prism 7. All statistical tests used an alpha value of 0.05 and were two-sided.

Results

Cohort characteristics

A total of 86 IBC patients with available pretreatment H&E-stained slides and who underwent mastectomy after NAC were identified in the IBC tumor registry and tissue bank. Baseline demographics, tumor characteristics, treatment regimens, and pathologic outcome data are shown in Table 1. Approximately 70% of cases had stage III disease with the rest having *de novo* stage IV disease; 90% had pure ductal histology with the remainder largely having mixed histology, and 70% of cases had grade III disease. HER2/neu-amplified ($HER2^+$) and hormone receptor–positive, HER2/neu nonamplified ($HR^+/HER2^-$) breast cancer receptor subtypes each represented 40% of the cohort population, and treatment regimens largely reflected this, with

Table 1. Cohort characteristics

	Full cohort ($n = 86$)	pCR ($n = 34$)	Non-pCR ($n = 52$)	*P* value
Age at diagnosis, mean years (range)	50 (23–75)	48 (23–64)	51 (27–75)	0.092
Race/ethnicity, *n* (%)				0.020
White	72 (83.7)	26 (76.5)	46 (88.5)	
Black	6 (7.0)	1 (2.9)	5 (9.6)	
Hispanic	7 (8.1)	6 (17.6)	1 (1.9)	
Asian	1 (0.1)	1 (2.9)	0 (0.0)	
Stage, *n* (%)				<0.001
Stage IIIB	32 (37.2)	12 (35.3)	20 (38.5)	
Stage IIIC	30 (34.9)	19 (55.9)	11 (21.2)	
Stage IV	24 (27.9)	3 (8.8)	21 (40.4)	
Receptor subtype, *n* (%)				0.019
TNBC	20 (23.2)	8 (23.5)	12 (23.1)	
$HER2^+$	34 (39.5)	19 (55.9)	15 (28.8)	
$HR^+/HER2^-$	32 (37.2)	7 (20.6)	25 (48.1)	
Histology, *n* (%)				1
Ductal	76 (88.4)	30 (88.2)	46 (88.5)	
Lobular	0 (0.0)	0 (0.0)	0 (0.0)	
Mixed	9 (10.5)	4 (11.8)	5 (9.6)	
Poorly differentiated	1 (0.1)	0 (0.0)	1 (1.9)	
Grade, *n* (%)				0.358
I	0 (0)	0 (0.0)	0 (0.0)	
II	28 (32.6)	9 (26.5)	19 (36.5)	
III	58 (67.4)	25 (73.5)	33 (63.5)	
Neoadjuvant treatment received				0.004
Anthracycline + taxane	29 (33.7)	4 (11.8)	24 (46.2)	
Taxane + anti-HER2 ± anthracycline or carboplatin	34 (39.5)	19 (55.9)	16 (30.8)	
Anthracycline + carboplatin + taxane + panitumumab	21 (24.4)	10 (29.4)	11 (21.2)	
Other (T-DM1, taxol+avastin)	2 (2.3)	1 (2.9)	1 (1.9)	

Abbreviations: pCR, pathologic complete response; TNBC, triple-negative breast cancer; $HER2^+$, HER2/neu-amplified breast cancer; $HR^+/HER2^-$, hormone receptor (estrogen receptor or progesterone receptor) positive, HER2/neu nonamplified breast cancer.

40% receiving anti-HER2–targeted regimens in combination with chemotherapy. During the time period over which this cohort was assembled, a clinical trial of carboplatin and panitumumab in combination with standard anthracycline- and taxane-based therapy (NCT01036087) was ongoing for patients with triple-negative breast cancer (TNBC) or $HR^+/HER2^-$ disease (22), and 25% of patients in this cohort received this treatment. Approximately 40% of patients experienced a pCR, and comparison of responders and nonresponders showed that the responder cohort was enriched with stage III patients and $HER2^+$ disease (Table 1). PFS was improved in patients experiencing a pCR in both the full cohort and when analyses were limited to patients with stage III disease (Supplementary Fig. S2A–S2B).

Characterization of immunologic aspects of the TME

The IBC TME was first interrogated by presenting stage and breast cancer receptor status (Fig. 1A–J; Supplementary Figs. S3A–S3Q, S4A–S4L, S5A–S5D, and S6A–S6J). Representative H&Es and stains are shown in Supplementary Fig. S3A–S3Q. Greater TIL frequencies were found in stage III disease compared with *de novo* stage IV disease ($P = 0.016$), and this was largely driven by the $HER2^+$ and TNBC subtypes (Fig. 1A; Supplementary Fig. S4H). Singlet IHC staining and multiplex IHC were performed to further characterize lymphoid and myeloid subsets (Fig. 1B–H; Supplementary Fig. S4A–S4E). Tumors from patients with stage III disease demonstrated higher lymphoid infiltrates ($CD8^+$, $CD56^+$, and $CD20^+$ cells) as well as HLA-DR, which is often seen on antigen-presenting cells as well as on activated lymphoid cells compared with *de novo* stage IV disease ($P = 0.010$, 0.062, 0.158, and 0.006, respectively). Differences in numbers of $CD8^+$ and $HLA\text{-}DR^+$ cells between IBC stages were largely seen in $HER2^+$ and TNBC subtypes; differences in $CD56^+$ cells were predominantly seen in $HR^+/HER2^-$ disease, and differences in $CD20^+$ cells primarily in TNBC (Supplementary Fig. S4I–S4L). Density of cells staining double positive for HLA-DR and CD68, CD163, or CD8 did not reveal any particular immune cell subset accounting for $HLA\text{-}DR^+$ cells being overrepresented in stage III disease (Supplementary Fig. S5A–S5D). Comparisons of receptor subtypes within stage III disease showed that $HER2^+$ disease had significantly higher numbers of $CD8^+$ cells compared with $HR^+/HER2^-$ disease ($P = 0.003$), and that TNBC had higher $CD20^+$ cells compared with $HR^+/HER2^-$ disease ($P = 0.027$; Fig. 1G–H; Supplementary Fig. S6A–S6H).

PD-L1 expression at $\geq$1% tumor cell positivity was demonstrated in only 1 of 43 cases (Supplementary Fig. 3E), and this case displayed only 1% staining. In contrast, approximately 30% of immune cells were positive for PD-L1 staining in this cohort but with no differences by stage or receptor subtype (Fig. 1I; Supplementary Fig. S4F).

To further characterize the specificity of the T-cell infiltrate, T-cell repertoire analysis was performed. No differences in T-cell clonality (reactivity) or T-cell richness (diversity) were seen by IBC stage or receptor subtype (Fig. 1J; Supplementary Figs. S4G and S6I–S6J).

TILs and mast cells are associated with response to neoadjuvant chemotherapy

We next asked if immune cell subsets were different between responders, defined as those experiencing pCR, and nonresponders (Fig. 2A–G; Supplementary Figs. S7A–S7J and S8A–S8M). Consistent with prior reports in non-IBC breast cancer, the presence of TILs was increased in the tumors of patients experiencing pCR ($P = 0.035$) with higher subsets of $CD8^+$ ($P = 0.047$) and $CD20^+$ cells ($P = 0.054$; Fig. 2A–C).

The immune marker most significantly associated with response was tryptase, a mast cell marker. Numbers of $tryptase^+$ cells were significantly higher in nonresponders than in responders ($P = 0.004$; Fig. 2D). Representative tryptase staining in nonresponder and responder cases is shown in Supplementary Fig. S3N and S3O, respectively. This association was seen in the full cohort, in stage III cases only, and also within each receptor subtype among the stage III cohort (Supplementary Fig. S8G). All other lymphoid and myeloid markers tested as well as PD-L1 and T-cell clonality and diversity metrics were not associated with response.

To further understand what immune interactions may account for this inverse relationship between mast cells and response, spatial assessment was performed on the multiplex myeloid panel (Fig. 2E–G). Focusing on 5 μm, 10 μm, and 20 μm distances between cells, within presumed range of interaction, we found that mast cells were within close proximity to $CD8^+$ T cells, $CD163^+$ macrophages, and tumor cells (as assessed by cytokeratin) in nonresponders compared with responders (Fig. 2H–J; Supplementary Fig. S7I–S7J), suggesting mast cells may be exerting immunosuppressive effects by interaction with these cell types in particular.

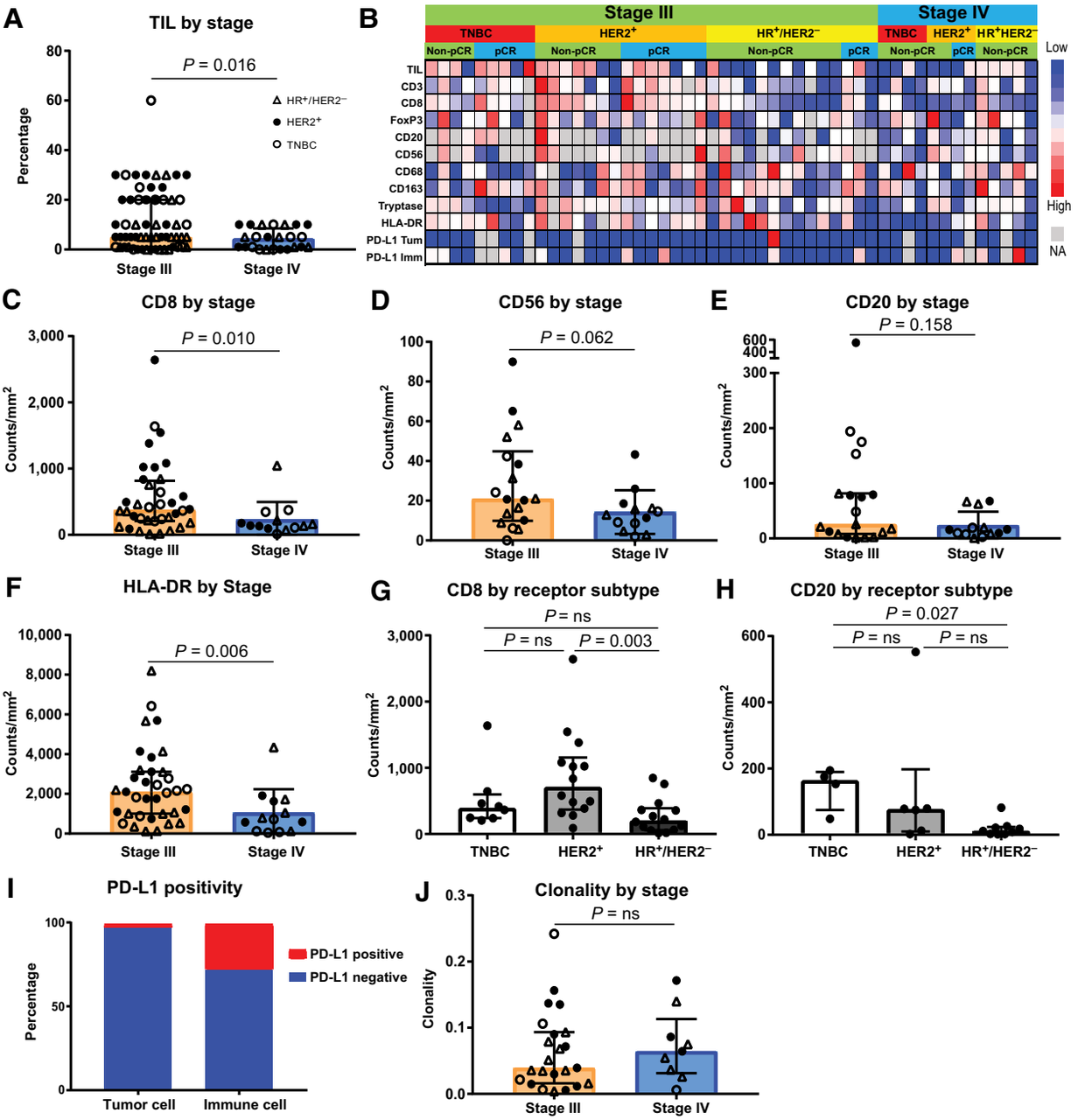

Figure 1.

Stage III IBC has a higher infiltrate of lymphoid cells and MHC class II presentation, whereas hormone receptor–positive disease has a lower lymphoid infiltrate. **A,** Quantification by TIL percentage of stromal area of primary breast tissue from stage III or *de novo* stage IV disease ($n = 62$ stage III and 24 stage IV patients). Receptor subtypes are denoted with triangle indicating hormone receptor positive, HER2/neu nonamplified ($HR^+/HER2^-$) disease, closed circle indicating HER2/neu-amplified ($HER2^+$) disease, and open circle indicating TNBC. **B,** Supervised clustering by stage, then receptor status and chemotherapy response of cases that received additional IHC immune assessment ($n = 37$ stage III and 13 stage IV patients). TIL percentage, CD3, CD8, FoxP3, CD20, CD56, CD68, CD163, tryptase, HLA-DR, and PD-L1 expression on tumor and immune cells are shown, with red indicating higher infiltration and blue lower infiltration. **C–F,** Quantification of $CD8^+$, $CD56^+$, $CD20^+$, and HLA-DR^+ cells by stage ($n = 36$ stage III and 13 stage IV, 18 stage III and 13 stage IV, 19 stage III and 13 stage IV, 35 stage III and 13 stage IV, respectively). **G** and **H,** Quantification of $CD8^+$ and $CD20^+$ cells by tumor receptor status ($n = 8$ TNBC, 14 $HER2^+$, 14 $HR^+/HER2^+$ for $CD8^+$, 4 TNBC, 6 $HER2^+$, 9 $HR^+/HER2^-$ for $CD20^+$ cells). **I,** Bar graph representing percentage of cases with PD-$L1^+$ tumors and immune cells ($n = 43$). **J,** TCR clonality by stage ($n = 23$ stage III and 9 stage IV). **A, C–H, J,** Bar heights indicate median values, and interquartile ranges are presented in addition to individual data points. All comparisons were made using two-sided Mann–Whitney *U* test (if two groups) or Kruskal–Wallis test with adjustment for multiple testing (if more than two groups).

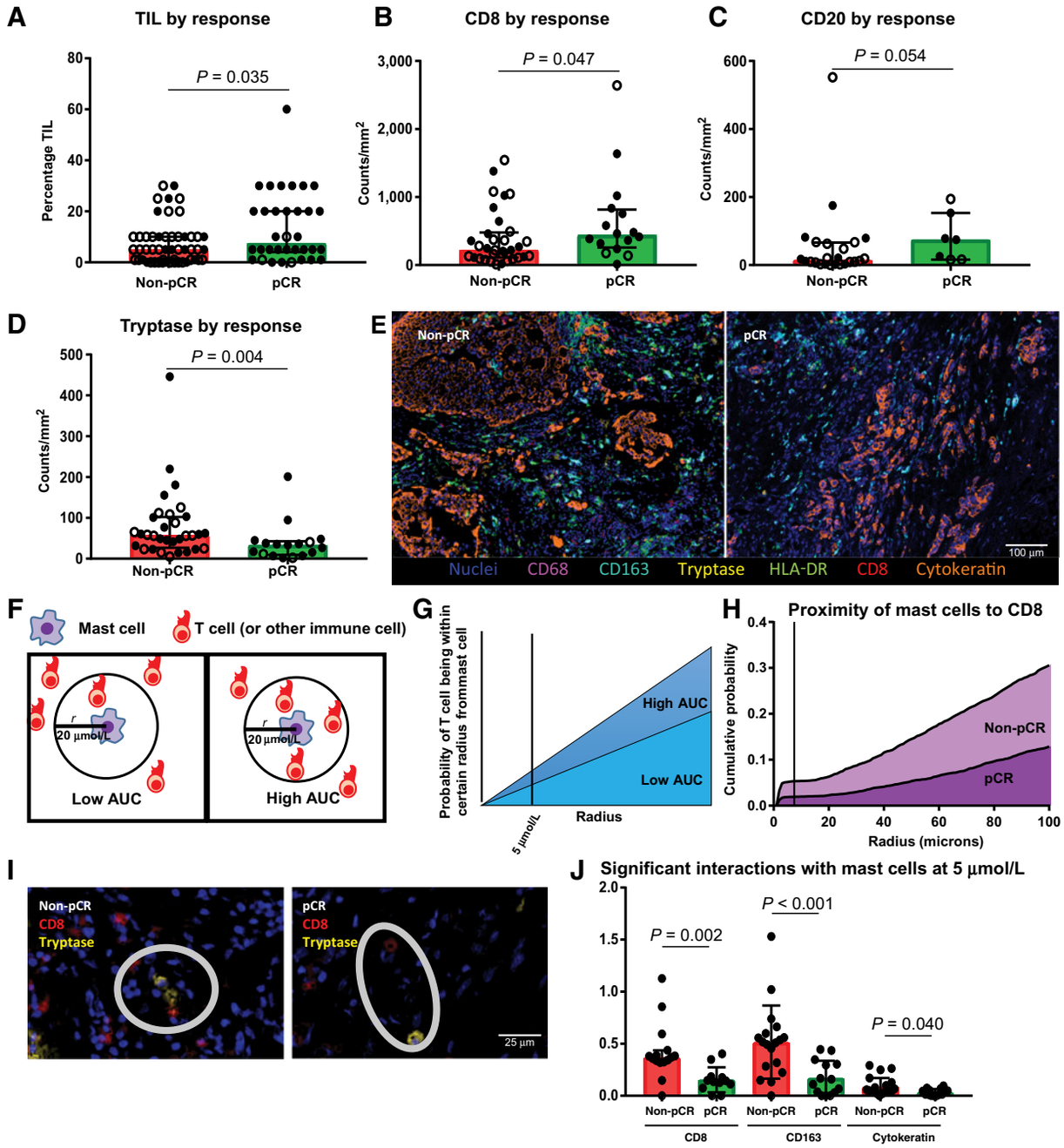

Figure 2.

Mast cells are the strongest immune predictor of poor response to chemotherapy, with higher TILs seen in responders than in nonresponders. **A–D,** TIL percentage and densities of $CD8^+$, $CD20^+$, and $tryptase^+$ cells by response, with response defined as achieving a pathologic complete response (pCR) or not (non-pCR; $n = 52$ non-pCR and 34 pCR, 33 non-pCR and 16 pCR, 24 non-pCR and 7 pCR, 32 non-pCR and 17 pCR, respectively). Closed circle indicates stage III cases, and open circle stage IV cases. **E,** Representative multiplex IHC image of a non-pCR and pCR case with nuclei (blue), CD68 (purple), CD163 (turquoise), tryptase (yellow), HLA-DR (green), CD8 (red), and cytokeratin (orange) stains depicted. **F** and **G,** Depiction of methodology for spatial analyses performed. Probabilities of a cell of interest being within a certain radius to another cell of interest were computed and area under the curve (AUC) calculated, with higher AUC indicating closer proximity. **H,** Non-pCR cases ($n = 15$) demonstrated higher AUC of mast cells to $CD8^+$ T cells than pCR cases ($n = 12$). **I,** Representative non-pCR and pCR cases showing distance between $CD8^+$ T-cell (red) and $tryptase^+$ mast cell (yellow). **J,** Comparisons by response of AUC between mast cells and $CD8^+$, $CD163^+$, and $cytokeratin^+$ (tumor) cells ($n = 15$ non-pCR and 12 pCR, 18 non-pCR and 14 pCR, 21 non-pCR and 14 pCR, respectively). **A–D, J,** Bar heights indicate median values, and interquartile ranges are presented in addition to individual data points. Comparisons were made using two-sided Mann–Whitney *U* test.

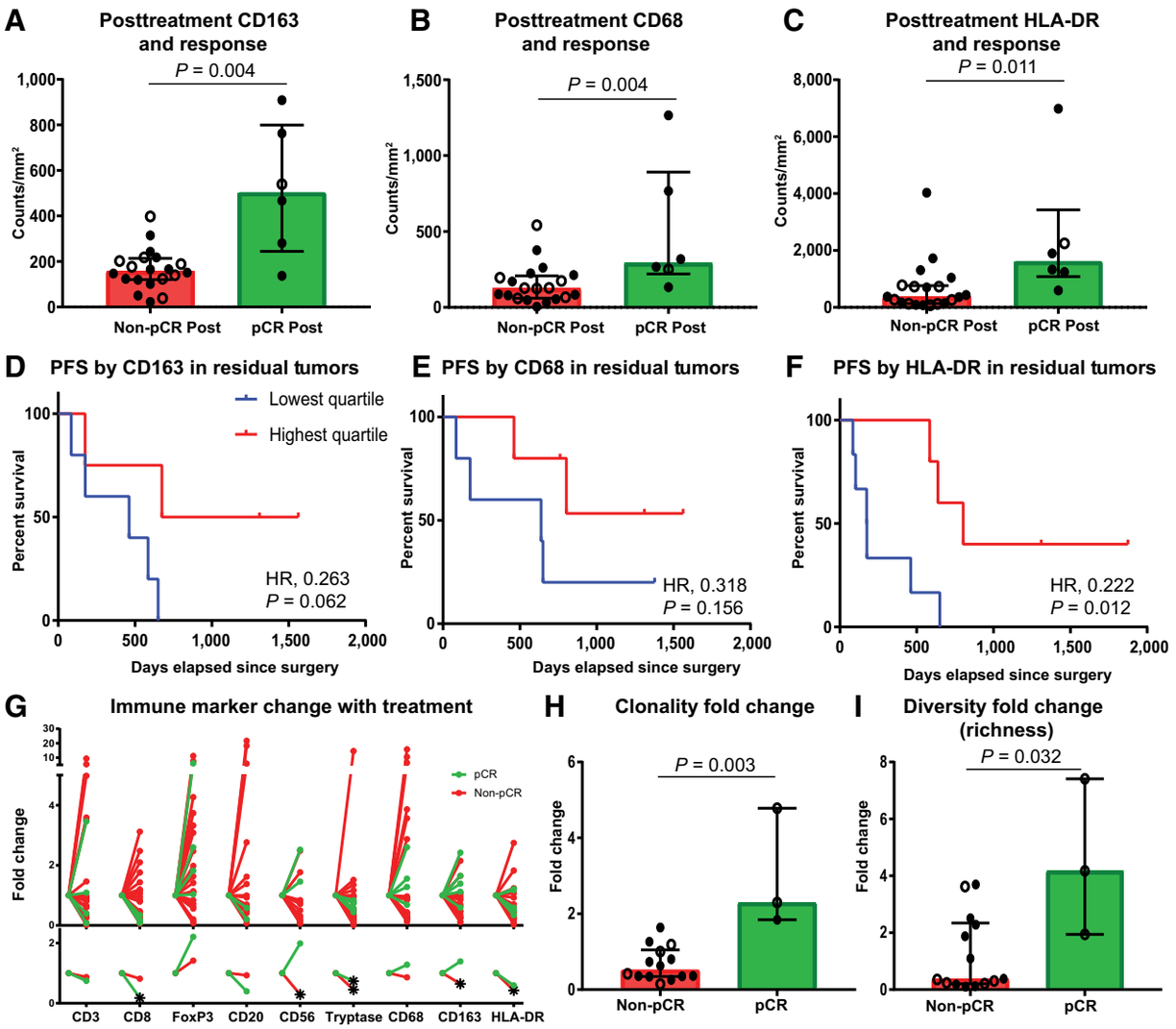

Figure 3.

Higher posttreatment myeloid cells are associated with improved outcomes. **A–C,** Densities of CD163$^+$, CD68$^+$, and HLA-DR$^+$ cells in the tumor bed at the time of mastectomy by response, with response defined as achieving a pathologic complete response (pCR) or not (non-pCR; $n = 20$ non-pCR and 6 pCR). **D–F,** Kaplan–Meier estimates of PFS from the time of surgery using two-sided log-rank test by residual densities of CD163$^+$, CD68$^+$, and HLA-DR$^+$ cells in residual tumor of non-pCR cases ($n = 20$). **G,** Immune marker fold change from baseline to mastectomy tumor bed of non-pCR (red) and pCR (green) cases for density of CD3$^+$ ($n = 19$ non-pCR and 4 pCR), CD8$^+$ ($n = 20$ non-pCR and 5 pCR), FoxP3$^+$ ($n = 19$ non-pCR and 4 pCR), CD20$^+$ ($n = 15$ non-pCR and 2 pCR), CD56$^+$ ($n = 14$ non-pCR and 2 pCR), tryptase$^+$ ($n = 18$ non-pCR and 5 pCR), CD68$^+$ ($n = 19$ non-pCR and 5 pCR), CD163$^+$ ($n = 19$ non-pCR and 5 pCR), and HLA-DR$^+$ ($n = 19$ non-pCR and 5 pCR) cells. Individual data points are depicted on the top, and median fold change on the bottom. Star indicates significant fold change from baseline, determined by one sample *t* test if variable normally distributed or Wilcoxon signed-rank test if not normally distributed by Shapiro–Wilk normality test. **H** and **I,** T-cell repertoire clonality and diversity fold changes from baseline to mastectomy tumor bed by response ($n = 14$ non-pCR and 3 pCR). **A–C, H** and **I,** Closed circle indicates stage III cases, and open circle indicates stage IV cases. Bar heights indicate median values, and interquartile ranges are presented in addition to individual data points. All comparisons were made using two-sided Mann–Whitney *U* test except where indicated.

Macrophages and MHC class II molecules are associated with improved PFS

On a subset of cases with available posttreatment tissue from their surgical specimen ($n = 27$), immune profiling was performed to characterize immune infiltrates in residual tumor as well as areas of treatment effect and to study the change in immune cells with therapy (Fig. 3A–F; Supplementary Figs. S9A–S9O and S10A–S10I). Pathologic response, stage, receptor subtype, and treatment characteristics of this cohort are provided in Supplementary Table S1. The cohort included tissue retrieved from the previous tumor bed in 6 patients who experienced a pCR and residual tumor in 21 patients who did not experience a pCR. Analysis of posttreatment tissue showed that myeloid infiltrates including macrophages, assessed by CD163 ($P = 0.004$) and CD68 ($P = 0.004$), as well as HLA-DR ($P = 0.011$), were present in significantly higher densities in the prior tumor bed

of cases that achieved a pCR compared with in the residual tumor of non-pCR cases (Fig. 3A–C). In addition, higher infiltration of these cell types was associated with improved PFS ($P = 0.062$, 0.156, and 0.012 for CD163, CD68, and HLA-DR, respectively) and a trend in improved OS among the non-pCR cases (Fig. 3D–F; Supplementary Fig. S10A–S10C). FoxP3$^+$ and CD56$^+$ cells were also elevated in pCR mastectomy tissue, whereas lower numbers of FoxP3$^+$ cells were associated with trend in improved OS among non-pCR cases (Supplementary Figs. S9C, S9E, and S10G).

When looking at fold change from pretreatment biopsy specimens to mastectomy specimens (Fig. 3G), there was a significant decrease in CD8$^+$ cells ($P < 0.001$) as well as tryptase$^+$ cell density ($P = 0.012$) with treatment in patients who experienced a pCR. Non-pCR cases also demonstrated a significant decrease in tryptase$^+$ cell density as well as in CD56, HLA-DR, and CD163 expression ($P = 0.021$, 0.049, 0.020, and 0.020, respectively). Fold change by treatment type is shown in Supplementary Fig. S11A, though it is difficult to draw conclusions on differential changes by therapy given the limited size of the cohort and that the pCR cases consisted of 5 patients who received anti-HER2–targeted therapy and 1 who received an EGFR inhibitor along with chemotherapy.

Treatment induces higher clonality as well as higher T-cell diversity in responders

T-cell repertoire analysis using TCR sequencing overall showed a significant change in repertoire with very low Morisita overlap values in both pCR and non-pCR cases (Supplementary Fig. S11B). Responders showed an increase in both clonality and diversity (richness) compared with nonresponder cases ($P = 0.003$ and 0.032, respectively; Fig. 3H and I).

Discussion

This study provides a large and comprehensive characterization of the IBC tumor immune microenvironment that has been performed using reliable methodology such as IHC to quantify immune cell subsets and determine their relationship to response. Mast cell infiltration, as identified by tryptase staining, was significantly associated with poor response to neoadjuvant chemotherapy in all stage and receptor subtypes of IBC and presents a possible therapeutic target.

Mast cells, which are known regulators of allergic and nonallergic inflammatory responses (23), are known to infiltrate breast cancer, but the literature has been inconsistent as to whether they are a favorable (24, 25) or poor prognostic indicator (26), with some data suggesting they may play different roles by breast cancer receptor subtype and grade (27, 28). This functional heterogeneity of mast cells may be a result of their ability to secrete a wide range of chemokines, growth factors, and other soluble mediators in a context-dependent fashion (29). Downstream effects therefore range from tumor promoting (stimulating angiogenesis/lymphangiogenesis, refs. 30, 31; extracellular matrix degradation, direct immunosuppression via secretion of TGFβ and IL10, and immune cell recruitment and activation of inhibitory cells such as myeloid derived suppressor cells and T regulatory cells) to tumor inhibiting (direct cytotoxic activity and immune cell recruitment and activation of cytotoxic T lymphocytes and other antitumor immune cells, ref. 32). In this cohort, in which mast cells were inversely associated with pCR across IBC subtypes, we explored potential immune interactions contributing to treatment resistance by analysis of spatial relationships with a multiplex IHC platform. By focusing on distances up to 20 μm (33), we found that mast cells were within range for direct or paracrine interactions with CD8$^+$ T cells, the primary effectors of antitumor responses, as well as CD163$^+$ macrophages and tumor cells. Mast cells may therefore at least partially be exerting their inhibitory effect in IBC through suppressing CD8$^+$ T cells, enhancing immunosuppressive CD163$^+$ macrophages, and directly promoting tumor cell growth. Prior studies support such interactions (34–39). Though this work will need to be validated with mechanistic studies, these data suggest mast cells may be a therapeutic target to enhance responses to NAC, and already existent agents such as mast cell stabilizers and c-Kit inhibitors make this readily translatable. In addition, these findings give further support that inflammation in "inflammatory" breast cancer extends beyond clinical appearance to underlying pathophysiology.

This study also demonstrated known lymphoid biomarkers of response to NAC as seen in non-IBC, including TILs (40), CD8$^+$ T-cell infiltrate (41), and CD20$^+$ B-cell infiltrate (42, 43), though notably these lymphoid infiltrates were less significantly associated with response compared with mast cell infiltration. Differences were noted in density of these lymphoid infiltrates by stage and by receptor status, with stage IV disease and hormone receptor–positive disease having a "colder" TME, therefore perhaps less immunogenic tumors than other subsets, potentially accounting for differential responses to therapy in these IBC subsets. Although lower TIL and specific lymphocyte subsets have previously been seen in matched primary metastases compared with primary breast cancer sites, this current study is unique in comprehensively characterizing primary breast tissue of *de novo* metastatic disease and showed that a less inflamed TME is seen at the site of the primary tumor and likely precedes development of distant metastases. PD-L1 positivity ($\geq$1%) was seen on tumor cells in only 1 of 43 pretreatment cases assessed and on immune cells in $\sim$30% of cases. Low PD-L1 positivity, in particular tumor cell positivity, is lower than seen in non-IBC even with the same antibody clone, suggesting this is not a primary mechanism for immune evasion in IBC (7, 44–49). Consistent with this, neither tumor nor immune cell PD-L1 positivity was correlated to response in this cohort. This rate of PD-L1 expression is consistent with prior RNA expression–based studies in IBC (11), and our IHC methodology additionally provides an accurate quantification of the number of cells with positive PD-L1 expression and further subdivides into tumor versus immune cell positivity. Unlike the prior report, our finding that PD-L1 is not predictive of pCR may reflect a more accurate characterization of PD-L1 expression though limited sample size may also be contributing.

Posttreatment tissue assessment revealed greater macrophage infiltration and HLA-DR staining in the prior tumor bed of patients experiencing a complete response to NAC as well as in residual tissue of non-pCR cases that had improved PFS. Interpretation of these findings is confounded by the overrepresentation of anti-HER2– and anti-EGFR–targeted treatments combined with NAC in the responders for the posttreatment cases available. Therefore, this may reflect that monoclonal antibody–treated patients demonstrate evidence of antibody-dependent phagocytosis, in which macrophages are critical effectors, and highlight

the importance of this mechanism in addition to NK cells in mediating improved outcomes (50, 51). As expected, higher NK cell infiltration was also seen with therapy in responders. In this limited cohort, no significant relationship was seen between lymphoid infiltration in residual tumor and PFS outcome, though greater numbers of FoxP3$^+$ cells were seen in pCR compared with non-pCR cases, perhaps again reflective of a trastuzumab treatment effect, as has been previously demonstrated (52); among the non-pCR cases, lower FoxP3$^+$ cell infiltration was associated with improved OS as previously reported in non-IBC (53). Analysis of change in T-cell repertoire dynamics showed that response was associated with an increase in clonality but also an increase in diversity metrics. This suggests that NAC (and again in this case monoclonal antibody and specifically HER2 targeted therapy) led to an increase in overall tumor reactive T cells as well as an increase in specific expanded T-cell clones accounting for increase in clonality. Similar to what was seen in pretreatment tissue, our cases were largely PD-L1–negative on tumor cells and positive in approximately one third of cases on immune cells, neither with correlation to survival outcome. Another study using tissue microarrays of 68 mastectomy IBC cases diagnosed prior to 2004 found that 37% of non-pCR cases were positive for PD-L1 on tumor cells and that this predicted worse survival (54); differences in the patient population (earlier stage patients and unknown neoadjuvant treatment characteristics in the other cohort), PD-L1 antibody clone used, and a limited sample size in our posttreatment cohort limit meaningful comparisons between these two studies. When comparing pCR and non-pCR cases, differences between cases in the area occupied by tumor cells in the residual tumor bed of non-pCR cases (vs. pCR cases for which there are no tumor cells present) may have added bias to our posttreatment results. However, the interspersed nature of IBC infiltration into the tissue made this difficult to account for. Nevertheless, the presence of consistent findings in our study between the pCR versus non-pCR tumor bed analysis and the survival analysis among non-pCR cases lends support for the accuracy and clinical relevance of our findings regarding higher macrophage infiltration and HLA-DR$^+$ cells in posttreatment tissue of responders. Our results will need to be validated in larger data sets with more homogenous populations by stage, receptor status, and associated therapies.

The primary limitation of this study is the relatively small size of the cohort and heterogeneity with respect to stage, receptor status, and associated differences in neoadjuvant treatments given. These mixed classes and treatment statuses therefore limit reliability of pooling data for pre- and posttreatment analyses. However, given the relative rarity of IBC and the comprehensive assessment of primary breast tissue from *de novo* IBC, the work presented here provides thorough immune characterization of IBC. To ensure accurate and robust conclusions from these data, all analyses were performed for the full cohort as well as within stage and receptor subsets when possible to determine both generalizable and subset-specific findings. These will need to be validated in additional IBC cohorts as well as compared with matched non-IBC to better understand the unique pathophysiology of IBC. In addition, with respect to our findings on mast cell infiltration predicting poor response to chemotherapy, mechanistic studies in addition to functional and activation profiling of the immune subsets (such as mast cells and CD8$^+$ T cells) are needed to further validate our findings and identify optimal modalities of therapeutically targeting IBC tumors.

In summary, this study provides a comprehensive immune profiling of IBC from which future studies can build. We showed expected biomarkers of response to NAC such as TILs and CD8$^+$ T-cell infiltrate, which have a known role across solid tumors in shaping response to therapy. We additionally identified mast cells as significantly associated with poor responses to therapy and a potential therapeutic target, highlighting the role of nonlymphoid subsets in IBC and perhaps even more generally the breast cancer TME. Together, these analyses provide an integrated profile of IBC to inform future design of IBC-specific clinical trials.

Disclosure of Potential Conflicts of Interest

V. Gopalakrishnan has received honoraria from the speakers bureau of the Kansas Society of Clinical Oncology and Excel CME, has ownership interest (including stock, patents, etc.) in UT MD Anderson Cancer Center, and is a consultant/advisory board member for MicrobiomeDX and ExpertConnect. M.T. Tetzlaff is a consultant/advisory board member for Novartis, LLC, Myriad Genetics, and Seattle Genetics. L.M. Coussens reports receiving commercial research grants from Acerta Pharma, LLC, Deciphera Pharmaceuticals, LLC, Roche Glycart AG, and Syndax Pharmaceuticals, Inc., reports receiving other commercial research support from Plexxikon Inc., Pharmacyclics, Inc., Acerta Pharma, LLC, Deciphera Pharmaceuticals, LLC, Genentech, Inc., Roche Glycart AG, Cell Signaling Technology, and NanoString Technologies, Inc., is a consultant/advisory board member for Pharmacyclics, Inc. steering committee for PCYC-1137-CA (NCT02436668), Syndax Pharmaceuticals, Inc. External Advisory Board, Cancer Research Institute (CRI), The V Foundation for Cancer Research, Cancer Research United Kingdom (CRUK) Early Detection (EDx) Research Committee, Starr Cancer Consortium, NIH/NCI-Frederick National Laboratory Advisory Committee (FNLAC), Cell Signaling Technology; Carisma Therapeutics Inc. Scientific Advisory Board, Verseau Therapeutics, Inc, Scientific Advisory Board, Zymeworks, Inc. Scientific Advisory Board, (P30) Melvin and Bren Simon Cancer Center, Indiana University, (P30) Koch Institute for Integrated Cancer Research, Massachusetts Institute of Technology, (P30) Salk Institute Cancer Center, Bloomberg–Kimmel Institute for Cancer Immunotherapy, Sidney Kimmel Comprehensive Cancer Center at Johns Hopkins, and Dana Farber Cancer Center Breast SPORE. A. Rao is a member of Voxel Analytics, reports receiving other commercial research support from Agilent Technologies, and is a consultant/advisory board member for Deoxylitics. N.T. Ueno reports receiving a commercial research grant from Amgen and Celgene. J.A. Wargo has received honoraria from the speakers bureau of Dava Oncology, Illumina, and PHE and is a consultant/advisory board member for Bristol-Myers Squibb, Novartis, Roche, Genentech, AstraZeneca, and Merck. E.A. Mittendorf is a consultant/advisory board member for Merck, Sellas Lifesciences, AstraZeneca, TapImmune, Peregrine Pharmaceuticals, and Genentech. No potential conflicts of interest were disclosed by the other authors.

Authors' Contributions

Conception and design: S.M. Reddy, M.T. Tetzlaff, A. Rao, W.A. Woodward, N.T. Ueno, S. Krishnamurthy, E.A. Mittendorf

Development of methodology: S.M. Reddy, A. Reuben, S. Barua, H. Jiang, T. Tsujikawa, L.M. Coussens, K. Wani, A. Rao, S. Krishnamurthy, E.A. Mittendorf

Acquisition of data (provided animals, acquired and managed patients, provided facilities, etc.): S.M. Reddy, A. Reuben, C.W. Hudgens, M.T. Tetzlaff, K. Wani, A. Wood, A. Rao, S. Krishnamurthy, J.A. Wargo, E.A. Mittendorf

Analysis and interpretation of data (e.g., statistical analysis, biostatistics, computational analysis): S.M. Reddy, A. Reuben, S. Barua, H. Jiang, S. Zhang, L. Wang, V. Gopalakrishnan, M.T. Tetzlaff, A. Rao, N.T. Ueno, S. Krishnamurthy, J.A. Wargo, E.A. Mittendorf

Writing, review, and/or revision of the manuscript: S.M. Reddy, A. Reuben, S. Barua, L. Wang, V. Gopalakrishnan, M.T. Tetzlaff, J.M. Reuben, A. Rao, W.A. Woodward, N.T. Ueno, S. Krishnamurthy, J.A. Wargo, E.A. Mittendorf

Administrative, technical, or material support (i.e., reporting or organizing data, constructing databases): S.M. Reddy, H. Jiang, Y. He, L. Villareal, A. Rao, N.T. Ueno, E.A. Mittendorf

Study supervision: S.M. Reddy, S. Krishnamurthy, E.A. Mittendorf
Other (wrote software modules for cell localization and spatial infiltration analysis): S. Barua
Other (spatial analysis, statistics): A. Rao

Acknowledgments

This research was funded by the Breast Cancer Research Foundation/Conquer Cancer Foundation Young Investigator Award (to S.M. Reddy), Breast Cancer Research Foundation (to N.T. Ueno), Morgan Welch Inflammatory Breast Cancer Research Program and Clinic, State of Texas Rare and Aggressive Breast Cancer Research Program Grant, and the MD Anderson Cancer Center Support grant (NCI #CA16672). S.M. Reddy received support from NIH T32 Training Grant T32 CA 009666. A. Reuben received support from the Kimberley Clark Foundation Award for Scientific Achievement provided by MD Anderson's Odyssey Fellowship Program. A. Rao received support from the CCSG Bioinformatics Shared Resource P30 CA016672, an Institutional Research Grant from The University of Texas MD Anderson Cancer Center, CPRIT RP170719, CPRIT RP150578, NCI R01CA214955-01A1, a Career Development Award from the MD Anderson Brain Tumor SPORE, a gift from Agilent technologies, and a Research Scholar Grant from the American Cancer Society (RSG-16-005-01). E.A. Mittendorf received support from the Pink Ribbons Project.

The costs of publication of this article were defrayed in part by the payment of page charges. This article must therefore be hereby marked *advertisement* in accordance with 18 U.S.C. Section 1734 solely to indicate this fact.

Received September 5, 2018; revised December 18, 2018; accepted April 22, 2019; published first May 1, 2019.

References

1. Robertson FM, Bondy M, Yang W, Yamauchi H, Wiggins S, Kamrudin S, et al. Inflammatory breast cancer: the disease, the biology, the treatment. CA Cancer J Clin 2010;60:351–75.
2. Masuda H, Brewer TM, Liu DD, Iwamoto T, Shen Y, Hsu L, et al. Long-term treatment efficacy in primary inflammatory breast cancer by hormonal receptor- and HER2-defined subtypes. Ann Oncol 2014;25:384–91.
3. Fouad TM, Kogawa T, Liu DD, Shen Y, Masuda H, El-Zein R, et al. Overall survival differences between patients with inflammatory and noninflammatory breast cancer presenting with distant metastasis at diagnosis. Breast Cancer Res Treat 2015;152:407–16.
4. Monneur A, Goncalves A, Gilabert M, Finetti P, Tarpin C, Zemmour C, et al. Similar response profile to neoadjuvant chemotherapy, but different survival, in inflammatory versus locally advanced breast cancers. Oncotarget 2017;8:66019–32.
5. Weiss A, Menen RS, Lin HY, Shen Y, Rosso KJ, Shaitelman S, et al. Factors associated with improved outcomes for metastatic inflammatory breast cancer patients. Breast Cancer Res Treat 2018;169:615–23.
6. Yan Y, Tang L, Tong W, Zhou J. The role and indications of aggressive locoregional therapy in metastatic inflammatory breast cancer. Sci Rep 2016;6:25874.
7. Nathan MR, Schmid P. The emerging world of breast cancer immunotherapy. Breast 2018;37:200–6.
8. Fouad TM, Kogawa T, Reuben JM, Ueno NT. The role of inflammation in inflammatory breast cancer. Adv Exp Med Biol 2014;816:53–73.
9. Mego M, Gao H, Cohen EN, Anfossi S, Giordano A, Tin S, et al. Circulating tumor cells (CTCs) are associated with abnormalities in peripheral blood dendritic cells in patients with inflammatory breast cancer. Oncotarget 2017;8:35656–68.
10. Lim B, Woodward WA, Wang X, Reuben JM, Ueno NT. Inflammatory breast cancer biology: the tumour microenvironment is key. Nat Rev Cancer 2018;18:485–99.
11. Bertucci F, Finetti P, Colpaert C, Mamessier E, Parizel M, Dirix L, et al. PDL1 expression in inflammatory breast cancer is frequent and predicts for the pathological response to chemotherapy. Oncotarget 2015;6:13506–19.
12. Bertucci F, Ueno NT, Finetti P, Vermeulen P, Lucci A, Robertson FM, et al. Gene expression profiles of inflammatory breast cancer: correlation with response to neoadjuvant chemotherapy and metastasis-free survival. Ann Oncol 2014;25:358–65.
13. Salgado R, Denkert C, Demaria S, Sirtaine N, Klauschen F, Pruneri G, et al. The evaluation of tumor-infiltrating lymphocytes (TILs) in breast cancer: recommendations by an International TILs Working Group 2014. Ann Oncol 2015;26:259–71.
14. Tsujikawa T, Kumar S, Borkar RN, Azimi V, Thibault G, Chang YH, et al. Quantitative multiplex immunohistochemistry reveals myeloid-inflamed tumor-immune complexity associated with poor prognosis. Cell Rep 2017;19:203–17.
15. Shapiro L. Connected component labeling and adjacency graph construction. Mach Intell Pattern Recognit 1996;19:1–30.
16. McAndrew A. An introduction to digital image processing with matlab notes for scm2511 image processing. School of Computer Science and Mathematics, Victoria University of Technology.; 2004.
17. Baddeley A. Analysing spatial point patterns in R. Technical report C, 2010. Version 4 [cited 2018 Jan 25]. Available from: https://research.csiro.au/software/r-workshop-notes.
18. Barua S, Fang P, Sharma A, Fujimoto J, Wistuba I, Rao AUK, et al. Spatial interaction of tumor cells and regulatory T cells correlates with survival in non-small cell lung cancer. Lung Cancer 2018;117:73–9.
19. Barua S, Solis L, Parra ER, Uraoka N, Jiang M, Wang H, et al. A functional spatial analysis platform for discovery of immunological interactions predictive of low-grade to high-grade transition of pancreatic intraductal papillary mucinous neoplasms. Cancer Inform 2018;17:1176935118782880.
20. Szmyt J. Spatial statistics in ecological analysis: from indices to functions. Silva Fenn 2014;48(1):1008.
21. Baddeley A, Turner R. spatstat: an R package for analyzing spatial point patterns. J Stat Softw 2005;12:1–42.
22. Matsuda N, Wang X, Lim B, Krishnamurthy S, Alvarez RH, Willey JS, et al. Safety and efficacy of panitumumab plus neoadjuvant chemotherapy in patients with primary HER2-negative inflammatory breast cancer. JAMA Oncol 2018;4:1207–13.
23. Theoharides TC, Alysandratos KD, Angelidou A, Delivanis DA, Sismanopoulos N, Zhang B, et al. Mast cells and inflammation. Biochim Biophys Acta 2012;1822:21–33.
24. Rajput AB, Turbin DA, Cheang MC, Voduc DK, Leung S, Gelmon KA, et al. Stromal mast cells in invasive breast cancer are a marker of favourable prognosis: a study of 4,444 cases. Breast Cancer Res Treat 2008;107:249–57.
25. Dabiri S, Huntsman D, Makretsov N, Cheang M, Gilks B, Bajdik C, et al. The presence of stromal mast cells identifies a subset of invasive breast cancers with a favorable prognosis. Mod Pathol 2004;17:690–5.
26. Amini RM, Aaltonen K, Nevanlinna H, Carvalho R, Salonen L, Heikkila P, et al. Mast cells and eosinophils in invasive breast carcinoma. BMC Cancer 2007;7:165.
27. Fakhrjou A, Naghavi-Behzad M, Montazeri V, Karkon-Shayan F, Norouzi-Panahi L, Piri R. The relationship between histologic grades of invasive carcinoma of breast ducts and mast cell infiltration. South Asian J Cancer 2016;5:5–7.
28. Glajcar A, Szpor J, Pacek A, Tyrak KE, Chan F, Streb J, et al. The relationship between breast cancer molecular subtypes and mast cell populations in tumor microenvironment. Virchows Arch 2017;470:505–15.
29. Frossi B, Mion F, Sibilano R, Danelli L, Pucillo CEM. Is it time for a new classification of mast cells? What do we know about mast cell heterogeneity? Immunol Rev 2018;282:35–46.
30. Mukai K, Tsai M, Saito H, Galli SJ. Mast cells as sources of cytokines, chemokines, and growth factors. Immunol Rev 2018;282:121–50.
31. Cimpean AM, Tamma R, Ruggieri S, Nico B, Toma A, Ribatti D. Mast cells in breast cancer angiogenesis. Crit Rev Oncol Hematol 2017;115:23–6.

32. Varricchi G, Galdiero MR, Loffredo S, Marone G, Iannone R, Marone G, et al. Are mast cells MASTers in cancer? Front Immunol 2017;8:424.
33. Carstens JL, Correa de Sampaio P, Yang D, Barua S, Wang H, Rao A, et al. Spatial computation of intratumoral T cells correlates with survival of patients with pancreatic cancer. Nat Commun 2017;8:15095.
34. Jachetti E, Cancila V, Rigoni A, Bongiovanni L, Cappetti B, Belmonte B, et al. Cross-talk between myeloid-derived suppressor cells and mast cells mediates tumor-specific immunosuppression in prostate cancer. Cancer Immunol Res 2018;6:552–65.
35. Wasiuk A, Dalton DK, Schpero WL, Stan RV, Conejo-Garcia JR, Noelle RJ. Mast cells impair the development of protective anti-tumor immunity. Cancer Immunol Immunother 2012;61:2273–82.
36. Jutel M, Watanabe T, Klunker S, Akdis M, Thomet OA, Malolepszy J, et al. Histamine regulates T-cell and antibody responses by differential expression of H1 and H2 receptors. Nature 2001;413:420–5.
37. Nagai Y, Tanaka Y, Kuroishi T, Sato R, Endo Y, Sugawara S. Histamine reduces susceptibility to natural killer cells via down-regulation of NKG2D ligands on human monocytic leukaemia THP-1 cells. Immunology 2012; 136:103–14.
38. Saleem SJ, Martin RK, Morales JK, Sturgill JL, Gibb DR, Graham L, et al. Cutting edge: mast cells critically augment myeloid-derived suppressor cell activity. J Immunol 2012;189:511–5.
39. Yang Z, Zhang B, Li D, Lv M, Huang C, Shen GX, et al. Mast cells mobilize myeloid-derived suppressor cells and Treg cells in tumor microenvironment via IL-17 pathway in murine hepatocarcinoma model. PLoS One 2010;5:e8922.
40. Denkert C, von Minckwitz G, Darb-Esfahani S, Lederer B, Heppner BI, Weber KE, et al. Tumour-infiltrating lymphocytes and prognosis in different subtypes of breast cancer: a pooled analysis of 3771 patients treated with neoadjuvant therapy. Lancet Oncol 2018;19:40–50.
41. Seo AN, Lee HJ, Kim EJ, Kim HJ, Jang MH, Lee HE, et al. Tumour-infiltrating $CD8^+$ lymphocytes as an independent predictive factor for pathological complete response to primary systemic therapy in breast cancer. Br J Cancer 2013;109:2705–13.
42. Brown JR, Wimberly H, Lannin DR, Nixon C, Rimm DL, Bossuyt V. Multiplexed quantitative analysis of CD3, CD8, and CD20 predicts response to neoadjuvant chemotherapy in breast cancer. Clin Cancer Res 2014;20:5995–6005.
43. Song IH, Heo SH, Bang WS, Park HS, Park IA, Kim YA, et al. Predictive value of tertiary lymphoid structures assessed by high endothelial venule counts in the neoadjuvant setting of triple-negative breast cancer. Cancer Res Treat 2017;49:399–407.
44. Nanda R, Chow LQ, Dees EC, Berger R, Gupta S, Geva R, et al. Pembrolizumab in patients with advanced triple-negative breast cancer: phase Ib KEYNOTE-012 study. J Clin Oncol 2016;34:2460–7.
45. Dirix LY, Takacs I, Jerusalem G, Nikolinakos P, Arkenau HT, Forero-Torres A, et al. Avelumab, an anti-PD-L1 antibody, in patients with locally advanced or metastatic breast cancer: a phase 1b JAVELIN solid tumor study. Breast Cancer Res Treat 2018;167:671–86.
46. Cimino-Mathews A, Thompson E, Taube JM, Ye X, Lu Y, Meeker A, et al. PD-L1 (B7-H1) expression and the immune tumor microenvironment in primary and metastatic breast carcinomas. Hum Pathol 2016;47:52–63.
47. Rugo HS DJ-P, Im S-A, Ott PA, Piha-Paul SA, Bedard PL, Sachdev J, et al. Preliminary efficacy and safety of pembrolizumab (MK-3475) in patients with PD-L1–positive, estrogen receptor-positive (ER+)/HER2-negative advanced breast cancer enrolled in KEYNOTE-028. [abstract]. In: Proceedings of the Thirty-Eighth Annual CTRC-AACR San Antonio Breast Cancer Symposium: 2015 Dec 8–12; San Antonio, TX. Philadelphia, PA: AACR; Cancer Res 2016;76:Abstract nr S5–07.
48. Pelekanou V, Barlow WE, Nahleh ZA, Wasserman B, Lo YC, von Wahlde MK, et al. Tumor-infiltrating lymphocytes and PD-L1 expression in pre- and posttreatment breast cancers in the SWOG S0800 phase II neoadjuvant chemotherapy trial. Mol Cancer Ther 2018;17:1324–31.
49. Hou Y, Nitta H, Wei L, Banks PM, Parwani AV, Li Z. Evaluation of immune reaction and PD-L1 expression using multiplex immunohistochemistry in HER2-positive breast cancer: the association with response to anti-HER2 neoadjuvant therapy. Clin Breast Cancer 2018;18:e237–e44.
50. Shi Y, Fan X, Deng H, Brezski RJ, Rycyzyn M, Jordan RE, et al. Trastuzumab triggers phagocytic killing of high HER2 cancer cells in vitro and in vivo by interaction with Fcgamma receptors on macrophages. J Immunol 2015; 194:4379–86.
51. Weiskopf K, Weissman IL. Macrophages are critical effectors of antibody therapies for cancer. MAbs 2015;7:303–10.
52. Muraro E, Comaro E, Talamini R, Turchet E, Miolo G, Scalone S, et al. Improved natural killer cell activity and retained anti-tumor CD8(+) T cell responses contribute to the induction of a pathological complete response in HER2-positive breast cancer patients undergoing neoadjuvant chemotherapy. J Transl Med 2015;13:204.
53. Ladoire S, Mignot G, Dabakuyo S, Arnould L, Apetoh L, Rebe C, et al. *In situ* immune response after neoadjuvant chemotherapy for breast cancer predicts survival. J Pathol 2011;224:389–400.
54. He J, Huo L, Ma J, Zhao J, Bassett RL, Sun X, et al. Expression of programmed death ligand 1 (PD-L1) in posttreatment primary inflammatory breast cancers and clinical implications. Am J Clin Pathol 2018;149:253–61.